JOURNAL OF MATERIALS SCIENCE **40** (2005) 2833–2836

Nucleation of stress-induced martensites in a Ti/Mo-based alloy

L. C. ZHANG, T. ZHOU, M. AINDOW*, S. P. ALPAY, M. J. BLACKBURN†
Department of Materials Science and Engineering, Institute of Materials Science, University of Connecticut, Storrs, CT 06269-3136, USA
E-mail: m.aindow@uconn.edu

M. H. WU
Memry Corporation, Bethel, CT 06801, USA

The formation of stress-induced α'' martensite in a metastable β Ti-Mo-based alloy has been studied using X-ray diffraction and transmission electron microscopy. The martensite nucleates heterogeneously at pre-existing sub-grain boundaries by dissociation of the boundary dislocations which bow out on inclined planes. The growth of martensite laths from the resultant stacking faults occurs by the motion of interfacial disconnections: the steps at the cores of these defects account for the apparent discrepancy between the {112} glide plane for the initial partial dislocation and the {334} habit plane for the martensite laths.

1. Introduction

The β-Ti alloys are an important class of structural materials because they exhibit an attractive combination of properties including high strength, low density and good corrosion resistance. These alloys contain transition metals such as Mo, V, Nb, W, Ta and Fe, which stabilize the bcc β phase and inhibit the transformation to the hcp α phase. The stability of the β phase in these alloys is frequently expressed as a Mo equivalent ($Mo_{eq.}$) in which the levels of other transition metal additions are weighted according to their potency [1]. Alloys with Mo equivalent values of ≈8–24 wt% are designated metastable β-Ti alloys because the transition metal content is high enough to prevent any martensitic transformation in the β phase upon quenching to room temperature [2]. Deformation of metastable β-Ti alloys can lead to the formation of stress-induced martensites (SIMs) [3–9]. Early studies on the structure of these martensites indicated a variety of possible products, including phases with hcp [3–5], bcc/bct [6] and hexagonal ω structures [8]. Subsequent studies [7, 9] revealed that these SIMs generally adopt a distorted hexagonal structure designated α'', which has an orthorhombic unit cell. It has been established that the orientation relationship (OR) between the β matrix and stressed-induced α'' product is approximately:

$$(11\bar{2})_\beta // (020)_{\alpha''}$$
$$[1\bar{1}0]_\beta // [001]_{\alpha''} \quad (1)$$

There is tremendous interest in such SIMs because they are the basis for the shape-memory and pseudoelastic effects. The crystallography of martensitic phases and the mechanisms by which they grow are reasonably well understood as a result of extensive theoretical analyses and experimental validation, primarily using transmission electron microscopy (TEM) [10, 11]. The mechanisms for the nucleation of martensitic transformations are, however, less well established, particularly for the thermoelastic martensites wherein the interface propagates extremely rapidly once nucleation has occurred. As such, it is difficult to capture the initial stages of their formation in TEM specimens. In this paper we present an X-ray diffraction (XRD) and TEM study on the early stages of martensitic formation in a metastable β Ti-Mo-based alloy. The implications of these observations for the nucleation and pseudoelastic deformation mechanisms in such alloys are discussed.

2. Experimental

An experimental alloy Ti-Mo-Nb-V-Al alloy was prepared by double vacuum arc melting and the final composition (in weight %), as measured using inductively coupled plasma optical emission spectrometry, was Ti–8.0 Mo–3.9 Nb–2.0 V–3.1 Al giving a $Mo_{eq.}$ value of 7.4 wt% [12]. The alloy button was hot-rolled to a final thickness of 1.3 mm and then solution-treated at 870°C in air, followed by air-cooling. Samples for tensile testing were then cut from the sheets and the sample surfaces were ground and polished to a final thickness of 0.8 mm. The testing was performed on an Instron model 5565 frame with appropriate extensometry, and a series of samples with final engineering strains, ε, of 1, 2, 3

*Author to whom all correspondence should be addressed.
†Professor Martin J. Blackburn died on March 12th 2004.

and 10% were produced. One sample was also tested to failure, which occurred at $\varepsilon \approx 14\%$. XRD spectra were obtained from the samples on a Bruker AXS D5005 diffractometer using Cu K_α radiation. The specimens for TEM studies were prepared by electropolishing to perforation using an electrolyte consisting of 6% perchloric acid, 34% butan-1-o1, and 60% methanol at -15°C followed by Ar^+ ion milling briefly at low voltage (1 kV) to remove any residual contamination on the sample surfaces. The deformation microstructures were analyzed in a Philips EM-420 TEM operated at 100 kV. High-resolution TEM (HRTEM) images were obtained in a JEOL 2010 FasTEM operating at 200 kV: this instrument is equipped with a high-resolution objective lens pole-piece (spherical aberration coefficient Cs = 0.5 mm) giving a point-to-point resolution of <0.19 nm in phase contrast image.

3. Results and discussion

XRD spectra were acquired over the angular range $2\theta = 33$–43° which includes the Bragg peaks for 110 from the β phase, and 110, 002 and 111 from the α'' martensite. The spectra from samples with $\varepsilon = 0$, 2 and 14% are shown in Fig. 1. The undeformed sample contained only the β phase as expected, and the value of the lattice parameter calculated from the peak positions was $a = 0.322$ nm. With increasing strain, a gradual splitting of the 110 β peak was observed until, for the broken sample ($\varepsilon = 14\%$), two peaks were observed: these were consistent with the 002 and 111 peaks for α'' martensite with lattice parameters $a = 0.301$ nm, $b = 0.491$ nm and $c = 0.453$ nm.

The microstructure of the broken sample was assessed by TEM and found to contain >80% by volume of α'' martensite which is consistent with our previous studies using optical microscopy [12]. Fig. 2a is a typical bright-field TEM micrograph showing thin pockets of retained β phase. Fig. 2b is the corresponding selected area diffraction pattern and is consistent with the OR given in (1) above.

To investigate the nucleation of the martensitic phase, the sample with $\varepsilon = 2\%$ was selected for subsequent TEM studies since this was the lowest strain at which there was clear XRD evidence for the presence of α'' martensite. It was found that, in this sample, almost all of martensite laths emanated from grain boundaries or sub-boundaries. One particularly informative example is shown in Fig. 3a. This is a bright field image of an

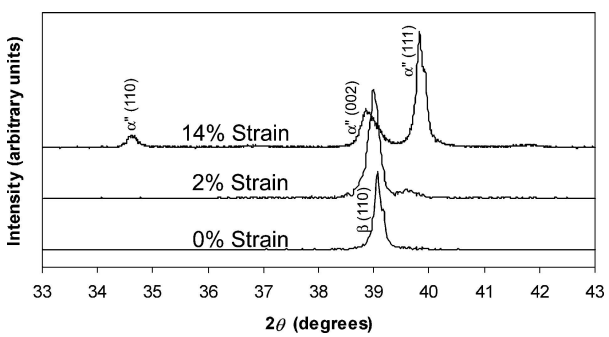

Figure 1 XRD spectra from the samples with $\varepsilon = 0, 2$ and 14% (broken).

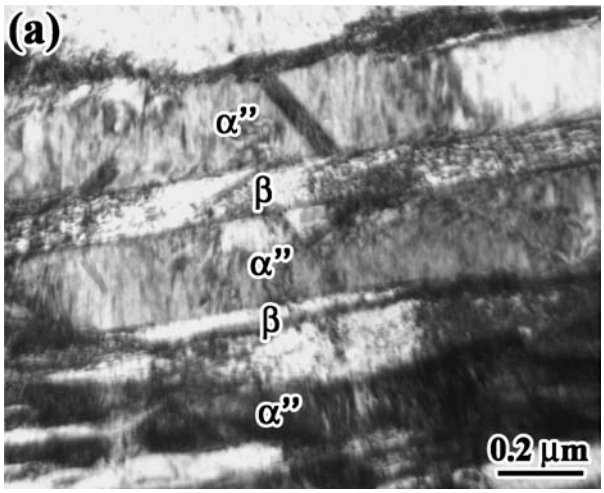

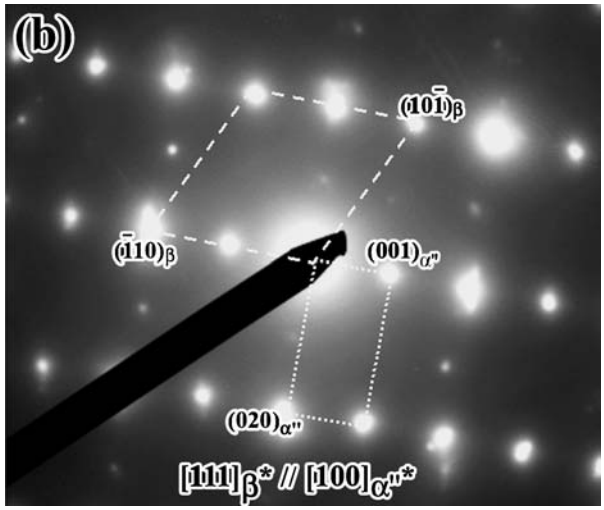

Figure 2 (a) Bright-field TEM micrograph and (b) corresponding $[111]_\beta$*//$[100]^*_{\alpha''}$ diffraction pattern obtained from the sample with $\varepsilon = 14\%$.

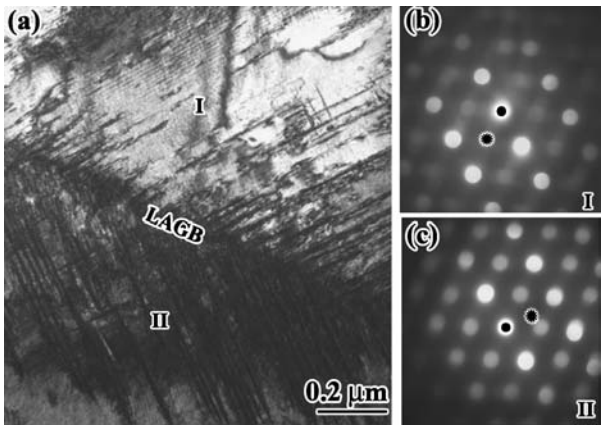

Figure 3 (a) Bright-field TEM micrograph from the sample with $\varepsilon = 2\%$, (b) & (c) micro-diffraction patterns from: (b) grain I; (c) grain II. In these patterns the dot indicates the direct beam whereas the asterisk corresponds to the position of the $[1\bar{1}0]_\beta$ zone axis as determined from the center of the intersecting Kikuchi bands.

area surrounding a low angle grain boundary (LAGB), in which martensite laths are found on different planes on either side of the boundary. Measurements of the displacement of Kikuchi band centers in micro-diffraction patterns obtained from the two grains (e.g. Figs 3b and c) revealed a misorientation of 1–2° across the LAGB.

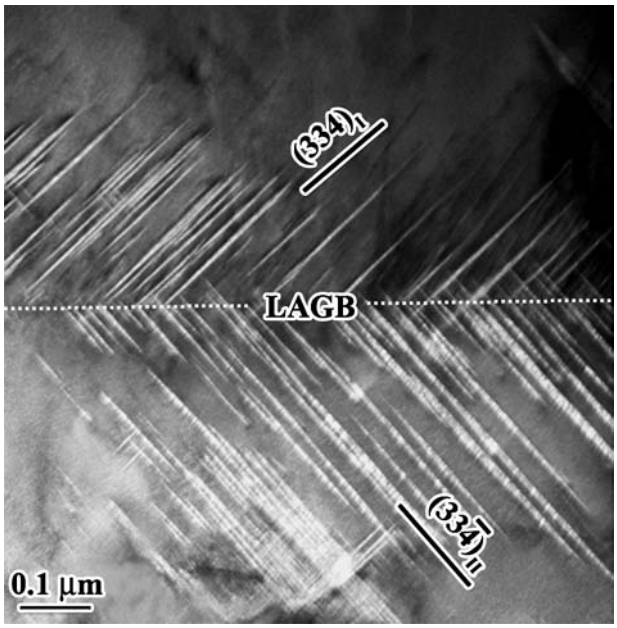

Figure 4 Dark-field TEM micrograph obtained from the region shown in Fig. 3 using $\mathbf{g} = 020_{\alpha''}$ with the beam direction close to the $[1\bar{1}0]_{\beta}//[001]_{\alpha''}$ zone axes.

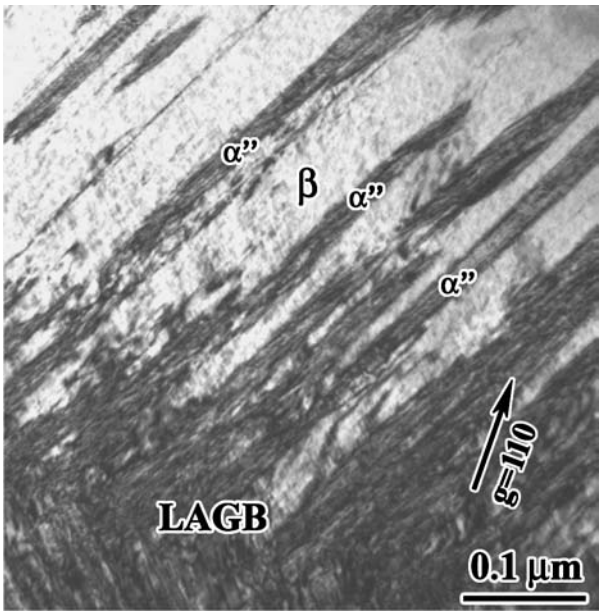

Figure 5 Bright-field TEM micrograph obtained from grain I in the region shown in Fig. 3 using $\mathbf{g} = 110$ with the beam direction close to $[1\bar{1}1]_{\beta}$.

We note that more accurate measurements were not possible due to distortions in the thin foil associated with the presence of the martensite laths.

The configuration of the martensite laths around the LAGB was revealed more clearly in dark field images such as Fig. 4, which was obtained using the 020 α'' reflection with the beam direction close to the $[1\bar{1}0]_{\beta}//[001]_{\alpha''}$ zone axes. The laths are lenticular with thicknesses of approximately 5–10 nm and aspect ratios of about 50. The habit planes for the laths are approximately edge-on in Fig. 4 and trace analysis was used to show that these are (334) and (33$\bar{4}$) in the upper and lower grains, respectively. This is consistent with the habit plane reported in the literature for α'' martensite in metastable β Ti-Mo-based alloy, and is close to that which one would expect for a Bain-type homogeneous invariant plane strain. In the latter case, the habit plane one would expect using the lattice parameters measured in this study is (3, 3, 3.743).

It was difficult to determine the details of the defect structures of the α''/β interfaces in diffraction contrast images because of the scale of the microstructure. The main characteristics are, however, revealed in images such as Fig. 5, which was obtained by tilting the interfaces in grain I until they were inclined at $\sim 45^{\circ}$ to the beam direction. It is clear that these interfaces contain arrays of line defects, which adopt a half-loop morphology near the lath tips. This implies that it is the motion of these defects that affects the growth of the martensitic laths. The dislocation character of these defects was assessed from such images using the $\mathbf{g}.\mathbf{b} = 0$ invisibility criterion and a partial analysis is shown in Fig. 6. The defects were out of contrast in images obtained using $\mathbf{g} = 112$ and $\mathbf{g} = 011$, which suggests that $\mathbf{b}$ for these defects is approximately parallel to $[11\bar{1}]$. A similar analysis of the interfacial defects in grain II gave $\mathbf{b}$ approximately parallel to [111]. It was not possible to evaluate the magnitude of $\mathbf{b}$ for these defects

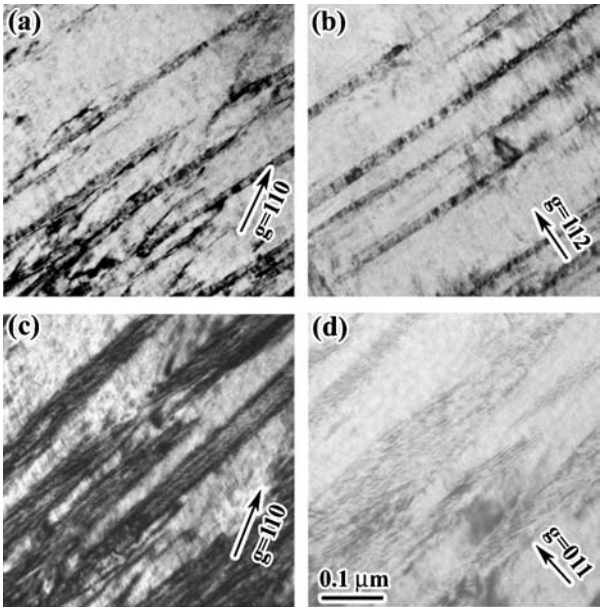

Figure 6 Bright field TEM micrographs obtained from grain I in the region shown in Fig. 3 using: (a) $\mathbf{g} = 110_{\beta}$ with the beam direction near $[1\bar{1}0]_{\beta}$, (b) $\mathbf{g} = 112_{\beta}$ with the beam direction near $[1\bar{1}0]_{\beta}$, (c) $\mathbf{g} = 110_{\beta}$ with the beam direction near $[1\bar{1}1]_{\beta}$, (d) $\mathbf{g} = 011_{\beta}$ with the beam direction near $[1\bar{1}1]_{\beta}$.

but clearly $\mathbf{b} \neq 1/2\langle 111 \rangle$ since these would be perfect dislocations in the bcc β phase and no change of crystal structure would be produced by their motion.

These observations are broadly consistent with a heterogeneous martensite nucleation mechanism, wherein dislocations in sub-grain boundaries dissociate under the influence of the applied stress and one of the partial dislocations bows out on a glide plane that is inclined to the boundary (e.g. [13]). The resultant faulted half-loop acts as a nucleus for the formation of a martensite lath, which grows by the passage of further partial dislocations on adjacent planes. If one of these defects were to pass over each atomic plane then the shear required to

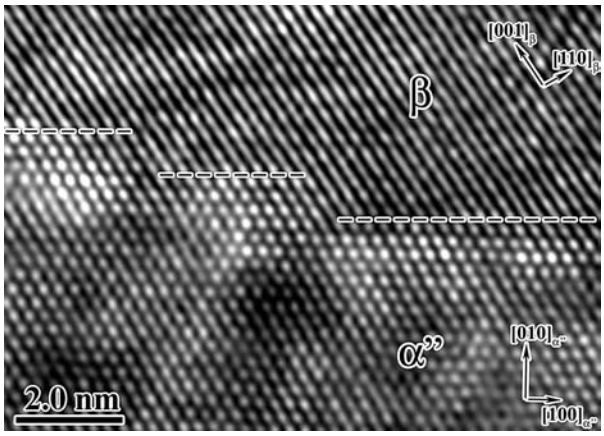

Figure 7 HRTEM image of an α''/β interface obtained with the beam direction parallel to the $[1\bar{1}0]_\beta//[001]_{\alpha''}$ zone axes.

produce the transformation from the β to the α'' structure would be $0.0417\langle 111\rangle$. The only problem with this model is that the habit plane of the resultant α'' lath would be {112}, i.e. parallel to the glide plane, not approximately {334} as measured experimentally. In the phenomenological theory of martensite crystallography such discrepancies are explained as the result of a lattice invariant deformation (LID), either twinning or dislocation glide, which modifies both the OR and habit plane. In the present case, however, the magnitude of the shear required is very small and the laths are so thin that the development of a LID is implausible.

The origins of this apparent discrepancy are revealed in HRTEM images such as Fig. 7 which was obtained from the interface of a lath in the upper grain in Fig. 4 with the beam direction parallel to the $[1\bar{1}0]_\beta//[001]_{\alpha''}$ zone axes. The lattice in the β phase is not revealed clearly in such images because the lattice spacing in the $[001]_\beta$ direction is below the point-resolution of the instrument. Nonetheless, such images do show clearly that the interface is corrugated with terraces parallel to (112), separated by an array of steps that give the average interface orientation of (334). No isolated defects were observed on any of the terraces and thus the defects observed in the diffraction contrast images such as Figs 5 and 6 must correspond to the steps. Interfacial defects with both dislocation and step character are described formally as disconnections [14]. As discussed in detail by Pond and Hirth [15], the Burgers vectors of such defects are given by combinations of symmetry operations, one from each of the adjacent crystals. For a disconnection on the α''/β interface with a step three atomic layers in height at its core, it can be shown that $\mathbf{b} = 0.1148\ \langle 1, 1, 1.2689\rangle$. The component of $\mathbf{b}$ parallel to $\langle 111\rangle$ is exactly equal to that required to produce the transformation from the β to the α'' structure (i.e. $0.1251\langle 111\rangle$). Moreover, for an array of these defects, the steps at the cores would rotate the habit plane away from {112} towards {334} as observed experimentally. Thus, all of the crystallographic features can be reconciled if the α'' martensite laths were to nucleate initially by the dissociation of dislocations in LAGBs and then grow by the passage of interfacial disconnections. A summary of the requirements for martensite growth by disconnection motion and a comparison of defect and phenomenological models for martensite transformations can be found in recent papers by Pond and co-workers [16, 17].

Finally, we note that the ability to capture these SIMs at such an early stage in their development implies that the α'' martensite is not thermoelastic, at least for this alloy composition. This supports our earlier contention that the formation of α'' martensite may not be the mechanism responsible for the pseudoelastic effect in Ti-Mo-based alloys [12].

4. Summary

A TEM study has been performed on nucleation of SIM in a metastable β Ti-Mo-Nb-V-Al alloy with a $Mo_{eq.}$ value of 7.4 wt%. The SIM exhibits the orthorhombic α'' structure and TEM observations of samples subjected to small tensile strains revealed that thin laths of this phase form first in the region adjacent to subgrain boundaries in the β phase. These laths lie on {334} planes and the α''/β interfaces contain arrays of defects with $\mathbf{b}//\langle 111\rangle$. It is inferred that these laths nucleate by the dissociation of dislocations in the boundaries with one of the partials bowing out on an inclined glide plane. Propagation of these laths occurs by the passage of interfacial disconnections with the steps at their cores giving the habit planes observed experimentally.

Acknowledgement

The authors would like to acknowledge Connecticut Innovations Inc. for financial support of this work.

References

1. P. BANIA, in "Beta Titanium Alloys in the 1990's," edited by D. Eylon *et al*. (TMS, Warrendale, PA, 1993) p. 6.
2. G. TERLINDE and G. FISCHER, in "Titanium '95 Science and Technology," edited by P. A. Blenkinsop, W. J. Evans, and H. M. Flower (University Press, Cambridge-UK, 1995) p. 2177.
3. M. HIDA, E. SUKEDAI, C. HENMI, K. SAKAUE and H. TERAUCHI, *Acta Metall.* **30** (1982) 1471.
4. M. K. KOUL and J. F. BEREDIS, *ibid.* **18** (1970) 579.
5. D. N. WILLIAMS, R. A. WOOD and E. S. BARTLETT, *Metall. Trans.* **3** (1972) 1529.
6. M. J. BLACKBURN and J. C. WILLIAMS, *Trans. TMS-AIME* **242** (1968) 2461.
7. T. W. DUERIG, G. T. TERLINDE and J. C. WILLIAMS, *Metall. Trans.* **A11** (1980) 1987.
8. T. S. KUAN, R. R. AHRENS and S. L. SASS, *ibid.* **A6** (1975) 1767.
9. T. W. DUERIG, J. ALBRECHT, D. RICHER and P. FISCHER, *Acta Metall.* **30** (1982) 2161.
10. G. B. OLSON and A. L. ROITBURD, in "Martensite: Martensitic Nucleation," edited by G. B. Olson and W. S. Owen (ASM International, Materials Park, OH, 1992) p. 149.
11. M. AHLERS, *Philos. Mag.* **A82** (2002) 1093.
12. T. ZHOU, M. AINDOW, S. P. ALPAY, M. J. BLACKBURN and M. H. WU, *Scripta Mater.* **50** (2004) 343.
13. M. COHEN, *Trans. Jpn. Inst. Metals* **29** (1988) 609.
14. J. P. HIRTH and R. C. POND, *Acta Mater.* **44** (1996) 4749.
15. R. C. POND and J. P. HIRTH, *Solid State Phys.* **47** (1994) 287.
16. R. C. POND and S. CELOTTO, *Int. Mater. Rev.* **48** (2003) 225.
17. R. C. POND, S. CELOTTO and J. P. HIRTH, *Acta Mater.* **51** (2003) 5385.

Received 17 November
and accepted 21 December 2004